RADIATION FLUX DISTRIBUTION OVER SOLAR IMAGES FORMED ON THE FOCAL PLANE BY A PARABOLOIDAL REFLECTOR WITH TRACKING ERRORS

Chang Shik HONG and Chai-sung LEE*

Department of Chemical Engineering, College of Engineering, Seoul National University, Seoul, Korea

(*Received 22 October 1986 • accepted 2 December 1986*)

Abstract—The radiation flux distribution of off-centered solar images formed by a sun-tracking paraboloidal reflector is theoretically analyzed for several tracking error angles using Jose's sunshape equation and assuming a specularly reflecting surface without taking meteorological conditions into consideration. The results are printed out by computer in the form of shade density maps to bring out a clear contrast to the low and high flux areas of a full image.

INTRODUCTION

Radiation flux analyses of the solar images thrown on the focal plane by paraboloidal reflectors have been studied by Jose [1], Harris and Duff [2] and others. Jose's work is particularly worthy of noting for his sunshape equation which he determined from studying the actually measured intensity data. His analysis, however, seems inconclusive in some area of the image by failing to give full account of all the contributions by the relevant beams contained in the reflected radiation cones. He also limited his analysis within the focal spot bounded by the image produced by the reflected cone from the vertex of the paraboloidal reflector.

Harris and Duff calculated the flux for a real surface. They incorporated the Jose's sunshape function with the idea of randomly varying surface normals whose deviations from the reference normal were characterized by a bivariate probability density function. This idea was originally proposed by Pettit [3] and also by Butler and Pettit [4]. Biggs and Vittitoe [5] proposed the use of a variable sunshape fuction to allow for the meteorological conditions in their flux calculations.

Recently, Look and Sundvold [6] introduced a procedure of calculating the radiative energy leaving a point source being reflected from one surface, and striking another. This procedure was applied to regular and extended parabolic and also circular cylindrical surfaces. The source radiation they used consisted simply of parallel beams with distributed wave lengths. In stead of probabilistic scattering of radiation by the surface, they took the reflectivity as a function of wave length.

None of the workers named above worked on obliquely incident radiations. In this work, we have been working on a two-dimensional sun-tracking system to orient a paraboloidal reflector towards the sun. The penumbra sun sensor mounted on the rim of the reflector has a resolution of 0.3 degrees, giving at least that much tracking error. Errors can be introduced in the assembling stage of the system due to machining errors and allowances. These errors will make the incident radiation oblique to the axis of the reflector. This work is proposed for analyzing the radiation flux on the focal plane when such radiations are reflected from a paraboloidal reflector. The tracking errors may be variable both in direction and in magnitude. They are likely to follow a certain pattern depending on the tracking system. Since this pattern is not known at this stage, we will choose several probable tracking error angles and concentrate ourselves in calculating the image flux density.

VECTOR REPRESENTATION

Visualize a paraboloidal reflector such as shown in Fig. 1. The dimensionless equation of a paraboloid can be written as

$$4\phi Z = X^2 + Y^2 \tag{1}$$

where ϕ is the dimensionless focal length f/R, and X, Y, and Z are the dimensionless coordinates x/R, y/R and z/R in the directions of x, y, and z, respectively. Suppose a point $O_i(X_i, Y_i, Z_i)$ on the reflecting surface, then, the radiation beam incident to and reflected from the point, as well as the normal to the paraboloid at the same point, can be expressed by vector notations $\vec{A}$, $\vec{B}$, and $\vec{P}$

* To whom all correspondence should be addressed

among which the relation below holds:

$$\vec{B} = -2(\vec{A}\cdot\vec{P})\vec{P} + \vec{A}. \tag{2}$$

Therefore, the incident vector $\vec{A}$, through reflection is transformed into vector $\vec{B}$, and this vector will intersect the focal plane, $Z = \phi$, at the point whose coordinates are:

$$X = X_i + (b_1/b_3)(\phi - Z_i),$$
$$Y = Y_i + (b_2/b_3)(\phi - Z_i),$$
$$\text{and } Z = \phi \tag{3}$$

where b_1, b_2 and b_3 are the X, Y and Z-directional components of the reflected unit vector $\vec{B}$.

Suppose that the angle formed between the incident radiation and the reflector axis is α as shown in the inset of Fig. 1, and the angle formed between the X-directional tangent at point O_i and the X-Y plane is δ, and that formed between the incident beam and the normal to the reflector surface at point O_i is ε, then, the energy δE_R that falls on a small area δS_R of the reflector at O_i can be expressed, if I_o is the incident intensity, by

$$\delta E_R = I_o \frac{\cos\varepsilon}{\cos\delta} \cdot \delta S_F \tag{4}$$

where δS_F is the projected area of δS_R on the X-Y plane. Denoting the unit vector in axial direction by $\vec{S}$,

$$\cos\varepsilon = -\vec{A}\cdot\vec{P}, \tag{5a}$$

$$\text{and } \cos\delta = \vec{S}\cdot\vec{P}. \tag{5b}$$

So far, the incident radiation on point O_i was treated

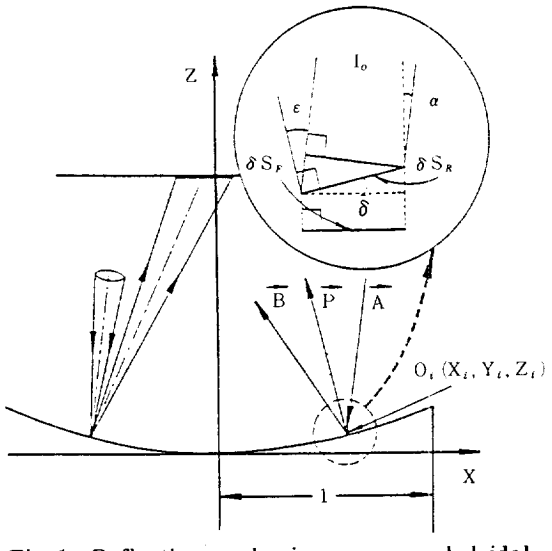

Fig. 1. Reflection mechanism on a paraboloidal reflector.

Inset shows the various angles and their geometrical relations.

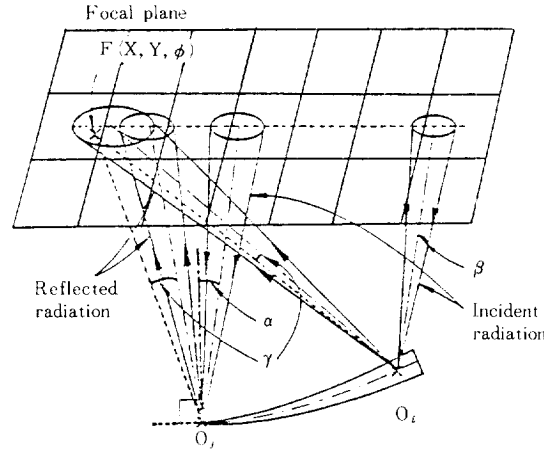

Fig. 2. Imaging mechanism on the focal plane.

as a single beam, while actually solar radiation falls on a point forming an inverted cone of light with an angle width of 0.53 degrees as shown by 2β in Fig. 2. Thus solar images are formed by reflected cones by being slantly intercepted by the focal plane. The images appear usually as somewhat distorted ellipses in shape instead of a point as is true in the case of parallel beams. Therefore, the brightness of the image, or the flux, at a point on the focal plane must be obtained by summing up the effects of all such reflected cones from all influential points on the reflector.

RADIATION FLUX ON THE FOCAL PLANE

In order to analyze the radiation flux on the focal plane, the following assumptions were postulated:

1. The radiation intensity of the apparent disk of sun is not uniform: it is distributed in accordance with the Jose's sunshape function.
2. The reflector surface is optically perfect and geometrically an ideal paraboloid.
3. Sun tracking is not perfect: the central beam of the incident radiation cone is slightly oblique to the axis of the reflector.
4. The conditions of the earth's atmosphere are the same as those of any fine days.
5. The reflector area shaded by the receiver is negligible.

The empirical equation of sunshape that Jose [1] presented is as follows:

$$I_c = \frac{R_c + 1.5641\sqrt{R_c^2 - r_c^2}}{2.5641\,R_c} I_{co} \tag{6}$$

where I_{co}, the intensity at the center of the cone, is determined as a function of R_c, the radius of the apparent

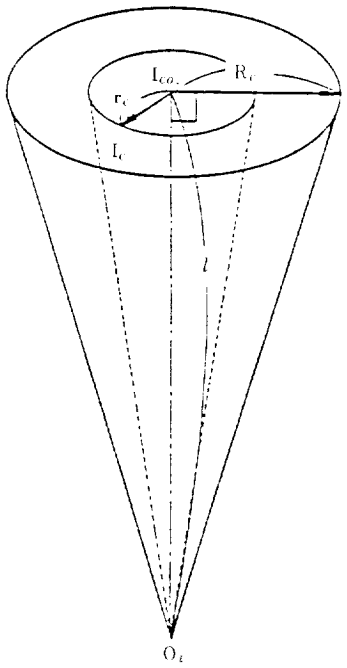

Fig. 3. Radiation cone of distributed intensity beams.

solar disk, and r_c is an arbitrary radius from the center of the cone on the same disk plane as shown in Fig. 3. Therefore, I_c represent the intensity at distance r_c from the center line of the cone. This is equivalent to the radius of the image of the solar disk formed on a plane which is perpendicular to the axis of a radiation cone reflected from a small area $\delta S_{R,i}$ at a point represented by O_i.

The energy $\delta E_{R,i}$ that is contained in the cone reflected from $\delta S_{R,i}$ is given by

$$\delta E_{R,i} = \int_0^{R_c} 2\pi r_c I_c dr_c \tag{7}$$

where $2\pi r_c dr_c$ is the increment of a concentric circular area of the image. Substituting eq. (6) into (7),

$$I_{co} = \frac{\delta E_{R,i}}{2.5028 R_c^2} \tag{8}$$

Introducing eq. (8) into (6),

$$I_c = \frac{R_c + 1.5641\sqrt{R_c^2 - r_c^2}}{6.4174 R_c^3} \delta E_{R,i} = G(R_c, r_c)\ \delta E_{R,i}. \tag{9}$$

This is the equation of intensity distribution of a radiation cone reflected from a small area $\delta S_{R,i}$ on the reflector.

Let δS be a small area at point F(X, Y, ϕ) within the

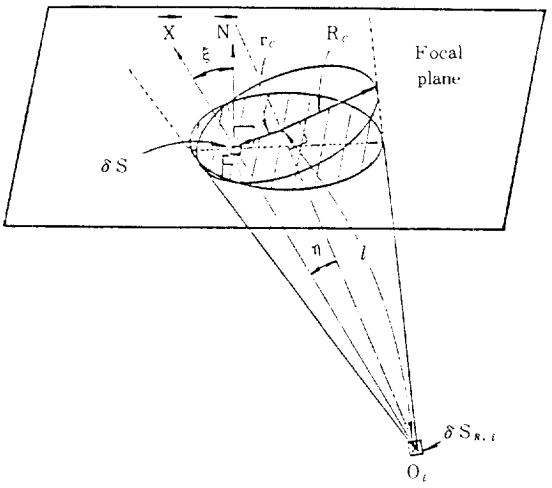

Fig. 4. A small area on the intercept of a reflected cone by the focal plane for which the flux calculation is to be made.

intercept of the reflected cone by the focal plane as shown in Fig. 4, and δE be the energy falling on that small area, then,

$$\delta E = I_c \cos\xi \cdot \delta S \tag{10}$$

where ξ is the angle between the normal to the focal plane at point F and the line connecting points F and O_i. The radiation flux at point F by the reflected radiation from point O_i can now be expressed by

$$\delta q_i = \frac{\delta E}{\delta S} = I_c \cos\xi. \tag{11}$$

Substituting eq. (9) into (11),

$$\delta q_i = G(R_c, r_c) \cos\xi \cdot \delta E_{R,i}. \tag{12}$$

Therefore, the radiation flux at point F that is contributed by the entire area of the reflector can be written by

$$q = \sum_i \delta q_i = \sum_i [G(R_c, r_c) \cos\xi \cdot \delta E_{R,i}] \tag{13}$$

where $\sum_i$ signifies summation of energies contributed by all the area elements $\delta S_{R,i}(i = 1,\infty)$ that reflect the radiation cones which throw lights on area δS at point F(note that not all points on the reflector contributes to this).

If the intensity of radiation incident on $\delta S_{R,i}$ is denoted by I_o as measured by a pyrheliometer, we can write, by recalling eq. (4), that

$$\delta E_{R,i} = I_o \frac{\cos\varepsilon}{\cos\delta} \delta S_{F,i} \tag{4b}$$

where $\delta S_{F,i}$ is the projection of $\delta S_{R,i}$ on the X-Y plane. Introducing eq. (4b) into (13) and converting the summa-

tion into integral form,

$$q=\int_{S_F} G(R_c, r_c)\frac{\cos\xi\cdot\cos\varepsilon}{\cos\delta} I_o dS_F \tag{14}$$

where

$$R_c = l\tan\beta, \tag{15}$$

and

$$r_c=\sqrt{(X-X_t)^2+(Y-Y_t)^2+(\phi-Z_t)^2-l^2}. \tag{16}$$

The integration must be carried out only within influential domains of S_F. Such domains should be determined as will be explained immediately after the following definitions.

Denoting the unit vector representing the normal to the focal plane by $\vec{N}(0,0,1)$ and the vector representing the radiation beam O_tF by $\vec{X}(X-X_t, Y-Y_t, \phi-Z_t)$, and taking the previously defined unit vector $\vec{B}(b_1, b_2, b_3)$ for the unit vector representing the central beam of the radiation cone reflected from point O_t, we can write that

$$\vec{X}\cdot\vec{B}=|\vec{X}|\cdot|\vec{B}|\cos\eta = l \tag{17}$$

and

$$\cos\xi = \frac{\vec{X}\cdot\vec{N}}{|\vec{X}|} \tag{18}$$

Because of the symmetry in the shape of a paraboloid, the infinitesimal area on its projected plane dS_F by Cartesian coordinates can be replaced by $rdrd\theta$ using angular coordinates. Thus, eq. (14) can be converted into the following form:

$$q=\int_{\theta_D}\int_{r_D} G(R_c, r_c)\frac{\cos\xi\cdot\cos\varepsilon}{\cos\delta} I_o r dr d\theta \tag{19}$$

where θ_D and r_D represent the integration ranges of angles and radii on the projected plane determined by choosing such values of θ and r on the corresponding reflector surface that the reflected radiation from such chosen points necessarily cast images over the designated point F on the focal plane.

COMPUTATIONAL PROCEDURES

When the central line of the incident radiation cone forms an angle α with the reflector axis, $\cos\varepsilon$ and $\cos\delta$ are expressed as follow:

$$\cos\varepsilon = -\frac{1}{\sqrt{r^2+4\phi^2}}(r\sin\alpha\cdot\cos\theta - 2\phi\cos\alpha), \tag{20}$$

$$\text{and}\quad \cos\delta = \frac{2\phi}{\sqrt{r^2+4\phi^2}} \tag{21}$$

where angle θ is measured counterclockwise on the X-Y plane from the the projection of the center line of the radiation cone incident on the center of the reflector.

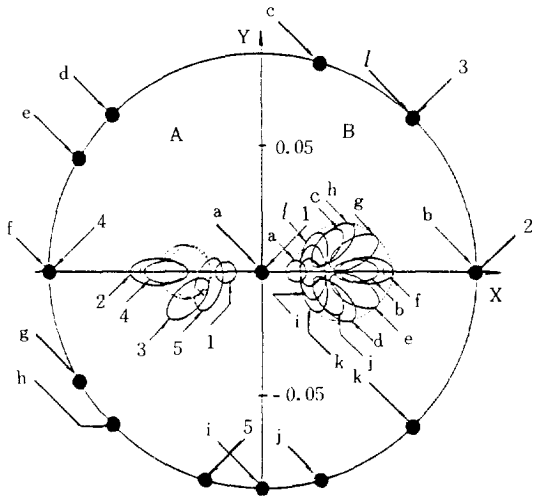

Fig. 5. Diagram showing separate θ-domains and an overall image boundary for an incident error angle of 1°.

The numbered 'ellipses' on the A-side of the focal plane correspond to the intercepts of radiation cones reflected at the same numbered points on the rim of the reflector whose size is drastically reduced because of space limitations. Note that intercepts 3 and 5 overlap partially in the neighborhood of point F (marked with x). The dotted lines are the locus of the center of intercepts of radiation cones from the rim of the reflector, 360° around. The B-side images show how an overall image boundary line (dotted) is formed. Refer to the alphabetically marked ellipses and points.

The value of the definite integral of eq. (19) can be determined by exploring for the effective domains indicated by θ_D and r_D. The r_D-domain can be found between 0 to 1, while the θ_D-domains may be found over one or more than one quadrants, in other words, they may consist of one or more than one separate domains on the projected reflector area as can be seen in Fig. 5. Any points (θ, r) on the reflector plane that cast images on point F on the focal plane are eligible for belonging to within the θ_D and r_D-domains. These points must satisfy the following weak inequality:

$$\cos\gamma \geqq \cos\beta \tag{22}$$

where (refer to Fig. 2)

$$\cos\gamma = \frac{1}{|\vec{X}|}[(kr\cos\theta - \sin\alpha)(X - r\cos\theta)$$

$$+krsin\theta\,(Y-rsin\theta)-(2k\phi+cos\alpha)\,(\phi-\frac{r^2}{4\phi})],$$

$$\vec{X}=(X-rcos\theta,\ Y-rsin\theta,\ \phi-\frac{r^2}{4\phi}), \tag{23}$$

and

$$k=\frac{2}{r^2+4\phi^2}\,(rsin\alpha\cdot cos\theta-2\phi cos\alpha). \tag{24}$$

Here, γ is the angle formed between $\vec{X}$ and $\vec{B}$, and β is the angle that subtends the radius of the apparent disk of the sun as before.

When the center line of the incident radiation cone is parallel to the reflector axis, we know that $\alpha=0$ from eqs. (20) and (21), and therefore, $\cos\varepsilon=\cos\delta$. This simplifies eq. (19) as follows:

$$q=\int_{\theta_D}\int_{r_D} G\,(R_c,\ r_c)\cdot cos\xi\cdot I_o\ rdrd\theta. \tag{25}$$

The integration of eqs. (19) and (25) were carried out numerically using the Romberg quadrature method [7]. The flow diagram for the computer programming procedure is shown in Fig. 6. The CPU time required for calculating for one focal plane point was 0.7 seconds by a VAX/VMS 750 system.

RESULTS AND DISCUSSIONS

The dimensions of paraboloid adopted in this work are as follow: aparture diameter, 106.68 cm; focal length, 45.75 cm; mirror radius r_r 61.28 cm; rim angle ϕ_r, 60.51°. The image size for zero dispersion, W, was calculated to be 1.1682 cm by the the following formula [8]:

$$W=\frac{2r_r\sin 16'}{\cos(\phi_r+16')} \tag{26}$$

Therefore, the dimensionless focal length, ϕ in eq. (1), is 0.8571.

Three different tracking error angles, such as 0°, 0.25° and 0.5° were assumed for the flux analyses on the focal plane. Flux analyses were also performed for such unlikely large angles as 1° and 3° to extend our study to the cases of poor tracking performance. Fig. 7 shows the shade density maps for solar images on the focal plane that were printed out by computer. Fig. 8 shows the relative sizes and positions of these images on

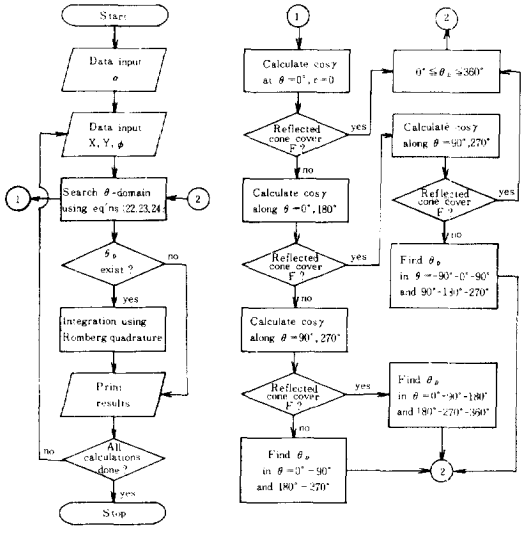

Fig. 6. Flow diagram for the computer programming for integration and domain explorations.

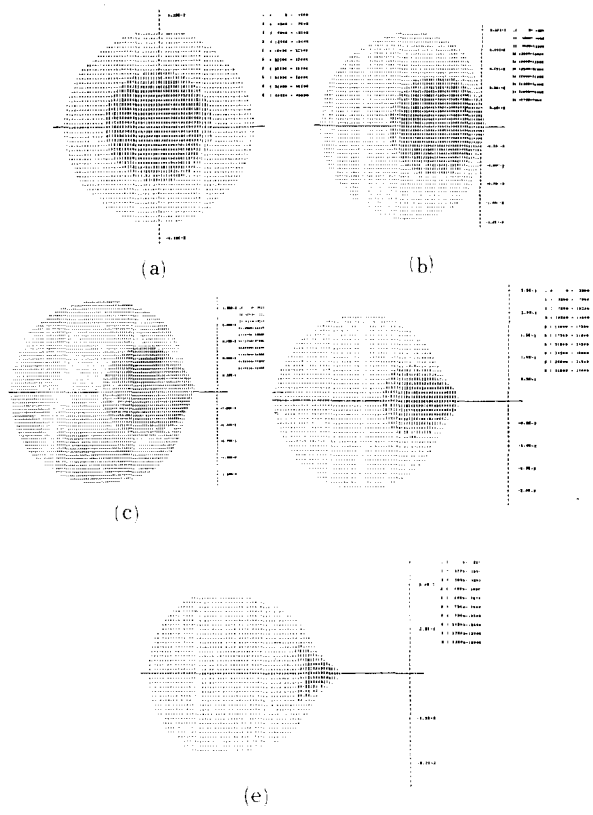

Fig. 7. Shade density maps for different tracking error angles.

(a) 0°, (b) 0.25°, (c) 0.5°, (d) 1° and (e) 3°. The values of the highest density for each of the five cases are 45,000, 45,000, 45,000, 34,000 and 15,000, respectively. The density is increased in 10 equal step by using synthesized prints.

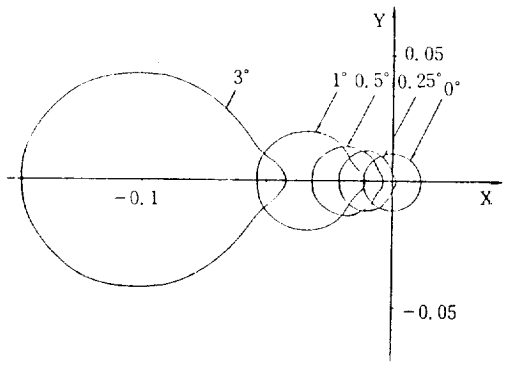

Fig. 8. Comparative sizes of images produced by incident radiation with different tracking error angles.

common coordinates, and Fig. 9 shows the vertical sectional diagram at Y = 0 showing the flux distribution on X-Z plane.

Each of the flux distribution maps in Fig. 7 (a, b, c, d, e) shows a characteristic dense spot which we may call by a 'hot spot'. The hot spots are surrounded by gradually less denser zones and then by sparse zones. It is no surprise to see that the hot spots and the surrounding intermediate zones tend to remain closer to the focal point while the sparse zones of the images tend to move to the left as the error angle is increased. It is also seen that the image as a whole is slightly compressed from both left and right in Fig. 7b and c, while in d and e, the images appear elongated in X-direction. The triangular deployment of the intermediate density points as in Fig. 7e is interesting to note because of the peculiar pattern the

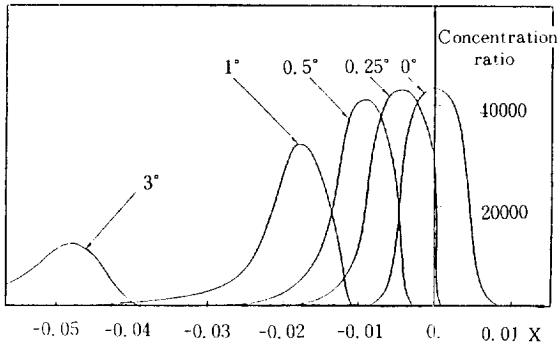

Fig. 9. Sectional view of flux distribution on X-Z plane at Y=0(flux in concentration ratio).

image assume.

It is possible to find out the intercept factor of a given sized flat receiver by referring to Fig. 8. However, the value found will serve as only a guide because the reflector surface being discussed here is not real. It is necessary to incorporate our procedure with a function charaterizing the real surface for the intercept factor to become practical.

CONCLUSION

When a paraboloidal concentrator is to be employed, one must first construct an efficient sun tracking device in order to avoid obliquely incident radiations. This work concentrated mainly on the computational method for handling obliquely incident radiations because complete elimination of tracking error is not possible. Here, we have established a method of calculating the radiation flux at an arbitrary point on the focal plane for any error angles. Same calculations were repeated to construct a shade density map which is equivalent to a flux distribution map. All numerical figures are based on dimensionless quantities to make the result general. Work is under way to extend our study to cover real surfaces.

REFERENCES

1. Jose, P.D.: The flux through the focal spot of a solar furnace. *Solar Energy* **1**(4), 17-22 (1957).
2. Harris, J.A. and Duff, W.S.: Focal plane flux distributions produced by solar concentrating reflectors. *Solar Energy*, **27**(5), 403-411 (1981).
3. Pettit, R.B.: Characterization of the reflected beam profile of solar mirror materials. *Solar Energy*, **19**, 733-741 (1977).
4. Butler, B.L. and Pettit, R.B.: Optical evaluation technique for reflecting solar concentrators. SPIE Vol. 114-Optics Applied to Solar Energy Conversion (1977).
5. Biggs, F. and Vittitoe, C.N.: The helios model for optical behavior of reflecting solar concentrators. Sandia Laboratories Energy Rep. SAND 76-0347 (1979).
6. Look, Jr. D.C. and Sundvold, P.D.: Analysis of concentrating collectors of energy from a distant point source. *Solar Energy*, **31**(6), 545-555 (1983).
7. Kuo, S.: "Computer Applications of Numerical Method", p. 282, Addison Wesley, London (1972).
8. Duffie, J.A. and Beckman, W.A.: "Solar Engineering of Thermal Processes", p. 291, John Wiley & Son, New York (1980).